A Novel Non-stationary Channel Model for UAV-to-Vehicle mmWave Beam Communications

Kai Mao[1], Qiuming Zhu[1(✉)], Maozhong Song[1(✉)], Benzhe Ning[1], Boyu Hua[1], Weizhi Zhong[2], and Xiaomin Chen[1]

[1] The Key Laboratory of Dynamic Cognitive System of Electromagnetic Spectrum Space, College of Electronic and Information Engineering, Nanjing University of Aeronautics and Astronautics, Nanjing 211106, China
{maokai,zhuqiuming,smz108,ningbenzhe,byhua,chenxm402}@nuaa.edu.cn

[2] The Key Laboratory of Dynamic Cognitive System of Electromagnetic Spectrum Space, College of Astronautics, Nanjing University of Aeronautics and Astronautics, Nanjing 211106, China
zhongwz@nuaa.edu.cn

Abstract. Taking into account of three dimensional (3D) trajectory, 3D antenna array, and 3D directional beam, a new unmanned aerial vehicle (UAV) to vehicle (U2V) millimeter wave (mmWave) channel model is proposed. Based on the propagation theory and ray tracing (RT) simulation results, the proposed U2V channel model is composed of a line-of-sight (LoS) path and three strongest non-line-of-sight (NLoS) paths or single-bounce (SB) paths. Meanwhile, considering the time-variant velocity and beam direction, the computation method of time-variant channel parameters, i.e., angles, delays, and powers, are also given and analyzed. The simulation results show that the statistical properties of proposed channel model, i.e., power delay profile (PDP) and power angle profile (PAP), are time-variant due to the non-stationarity of U2V propagation environment. Moreover, the simulated autocorrelation function (ACF) fits well with the theoretical one as well as the measured one, which validates the correctness of proposed model.

Keywords: U2V mmWave channel · Non-stationary channel · Channel model · 3D trajectory · 3D beam

1 Introduction

The fifth-generation (5G) or beyond 5G (B5G) mobile communication system is expected to provide high transmission rate and connect everything, where the UAV has been considered a promising component as the flying base station or flexible relay [1,2]. However, different with traditional mobile communication scenarios, the UAV flies in the 3D space with 3D trajectory and 3D-shaped

M. Guan and Z. Na (Eds.): MLICOM 2020, LNICST 342, pp. 471–484, 2021.
https://doi.org/10.1007/978-3-030-66785-6_51

antenna array. Moreover, to compensate the high path loss caused by mmWave band, the 3D beam-forming technologies are usually adopted in UAV mmWave communications [3,4]. These new features would affect channel characteristics significantly and make the traditional mobile channel models unsuitable [5,6]. Therefore, it is vital to deeply understand the UAV mmWave beam channel for the system design, algorithm optimization, and performance evaluation of U2V communication systems.

Several UAV channel models for sub-mmWave can be addressed in [7–13]. These models have considered part of new features, e.g., 3D scattering environment or 3D trajectory by upgrading the traditional deterministic channel models (DCMs) or geometry-based stochastic models (GBSMs), but they were not applicable for the mmWave band. For the existing mmWave channel models, most of them focused on the land mobile communication scenarios [14–22], and only a few involved the UAV mmWave scenario [23–26].

The authors in [23,24] used the RT method to simulate huge amount data of UAV mmWave channel and analyzed the characteristics of channel parameters, i.e., received power, path delay and propagation angle. However, the basic channel model was 2D in [23] and the ground station was fixed in [24]. The authors in [25] analyzed the 2D UAV mmWave channel characteristics by field test in an anechoic chamber. In [26], the authors proposed a 3D UAV-to-ground mmWave channel based on the GBSM method, but the velocity of UAV was constant and the ground station is also fixed. Recently, a 3D mmWave UAV channel model allowing time-variant arbitrary trajectory was proposed in [27], but the authors ignored the factor of 3D-shaped antenna rotation and beam-forming. This paper aims to fill this gap. The major contributions and novelties are summarized as follows:

1) A 3D U2V mmWave beam channel model considering the 3D arbitrary trajectory, 3D antenna array, and 3D directional beam is proposed. Based on the RT data and directional beam characteristics, the new model consists of a LoS path and three strongest NLoS paths to achieve the tradeoff between complexity and precision.
2) A deterministic and stochastic mixed computation method of channel parameters for the proposed model is developed. The deterministic channel parameters, e.g., powers, angles, and delays, are calculated by the time-variant geometric relationship, and the stochastic channel parameters, e.g., the angles and delays of rays are generated randomly based on the distribution obtained by the RT method.
3) Considering a typical U2V mmWave communication scenario, the channel parameters, i.e., angles, delays, and powers, are simulated and analyzed. Moreover, the statistical properties of ACF and Doppler power spectral density (DPSD) are also simulated and validated by theoretical and measured ones.

The rest paper is organized as follows. In Sect. 2, a 3D U2V mmWave beam channel model is proposed. Section 3 gives the hybrid computation method of channel parameters. The simulation and analytical results of channel parameters

and statistical properties are conducted in Sect. 4. Finally, conclusions are drawn in Sect. 5.

2 U2V mmWave Beam Channel Model

Let us consider the down link of U2V communication system, where the UAV adopts the 3D beam-forming to compensate the high path loss and the vehicle is equipped with omnidirectional antennas as shown in Fig. 1. In the figure, there are two local coordinate systems denoted as the UAV coordinate system and vehicle coordinate system with their origins at the central position of UAV and vehicle, respectively. Under the realistic condition, the UAV and vehicle travel with 3D arbitrary velocities as

$$\mathbf{v}_{\mathrm{rx/tx}}(t) = \left\|\mathbf{v}_{\mathrm{rx/tx}}(t)\right\| \begin{bmatrix} \cos\beta^{v}_{\mathrm{rx/tx}}(t)\cos\alpha^{v}_{\mathrm{rx/tx}}(t) \\ \cos\beta^{v}_{\mathrm{rx/tx}}(t)\sin\alpha^{v}_{\mathrm{rx/tx}}(t) \\ \sin\beta^{v}_{\mathrm{rx/tx}}(t) \end{bmatrix} \tag{1}$$

where $\left\|\mathbf{v}_{\mathrm{tx/rx}}(t)\right\|$ is the amplitude of $\mathbf{v}_{\mathrm{tx/rx}}(t)$, $\alpha^{v}_{\mathrm{tx/rx}}(t)$ and $\beta^{v}_{\mathrm{tx/rx}}(t)$ are the travel direction of UAV and vehicle on the azimuth and elevation plane, respectively. Moreover, the location vectors of UAV transmitting antenna and vehicle receiving antenna in their own coordinate systems can be denoted as $\mathbf{d}_{\mathrm{tx/rx}}(t) = [d^{x}_{\mathrm{tx/rx}}(t), d^{y}_{\mathrm{tx/rx}}(t), d^{z}_{\mathrm{tx/rx}}(t)]$. During the movement of UAV and vehicle, the location of each antenna may change and this paper introduces a rotation matrix $\mathbf{R}_{\mathrm{tx/rx}}(t)$ to take this factor into account

$$\mathbf{R}_{\mathrm{tx/rx}}(t) = \begin{bmatrix} \cos\beta^{v}_{\mathrm{tx/rx}}(t)\cos\alpha^{v}_{\mathrm{tx/rx}}(t) & -\sin\alpha^{v}_{\mathrm{tx/rx}}(t) & -\sin\beta^{v}_{\mathrm{tx/rx}}(t)\cos\alpha^{v}_{\mathrm{tx/rx}}(t) \\ \cos\beta^{v}_{\mathrm{tx/rx}}(t)\sin\alpha^{v}_{\mathrm{tx/rx}}(t) & \cos\alpha^{v}_{\mathrm{tx/rx}}(t) & -\sin\beta^{v}_{\mathrm{tx/rx}}(t)\sin\alpha^{v}_{\mathrm{tx/rx}}(t) \\ \sin\beta^{v}_{\mathrm{tx/rx}}(t) & 0 & \cos\beta^{v}_{\mathrm{tx/rx}}(t) \end{bmatrix}. \tag{2}$$

Considering the U2V communication, the propagation channel can be modeled as the combination of LoS part $H^{\mathrm{LoS}}(\tau, t)$ and NLoS part $H^{\mathrm{NLoS}}(\tau, t)$. The LoS part contains one direct path while the NLoS part contains several non-direct paths with different delays, e.g., SB, double bounce, etc. Thus, the total channel impulse response (CIR) between the *pth* UAV antenna and *qth* vehicle antenna scaled by the K-factor K_R can be expressed as

$$H_{p,q}(\tau, t) = \sqrt{\frac{K_R(t)}{K_R(t)+1}} H^{\mathrm{LoS}}(t) + \sqrt{\frac{1}{K_R(t)+1}} H^{\mathrm{NLoS}}(\tau, t). \tag{3}$$

In order to achieve the tradeoff between complexity and precision, we have performed huge number of simulations by RT method on the U2V mmWave channel under different scenarios. The simulated results show that the LoS path and ground specular (GS) path usually exist, and the powers of GS path and 1^{st} SB path are 20–30 dB below the one of LoS path. Moreover, the power of 2^{st} SB path has much lower power, e.g., below 60 dB, comparing with the one of 1^{st}

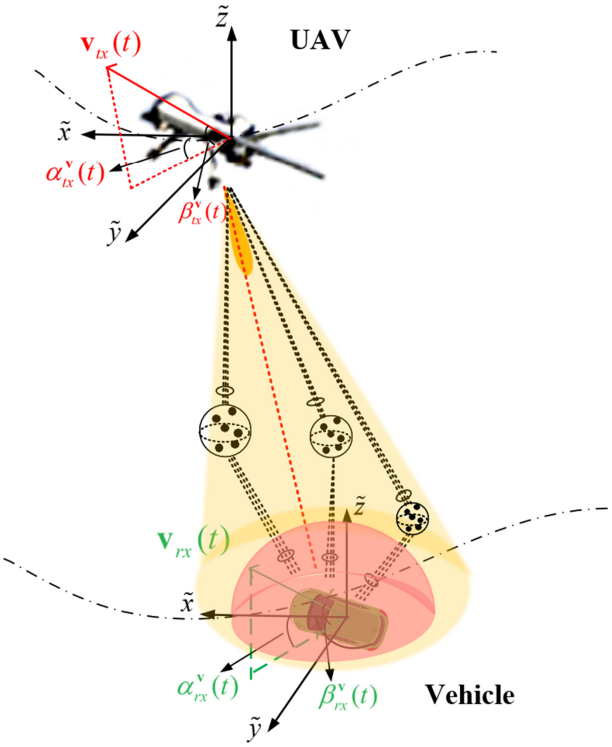

Fig. 1. Typical U2V communication scenario.

SB path. Based on these results, this paper only takes the GS and two strongest SB paths into the NLoS part as

$$H^{\mathrm{NLoS}}(\tau,t) = \underbrace{H^{\mathrm{GS}}(\tau,t)}_{ground\ specular} + \underbrace{H^{\mathrm{SB_1}}(\tau,t)+H^{\mathrm{SB_2}}(\tau,t)}_{Single\ bounce} \tag{4}$$
$$= \sum_{j=1}^{3}\sum_{m=1}^{M} h_m^j(t)\delta(t-\tau_m^j(t)),\ j=\{GS,\ SB_1, SB_2\}$$

where M is the valid ray number of each path, $h_m^j(t)$ and $\tau_m^j(t)$ are the channel coefficient and delay of mth ray within the GS and SB paths, respectively. Furthermore, the channel coefficient is modeled by the summation of several rays (or sub-paths) as

$$h_m^j(t) = \exp(\mathrm{j}\Phi_m)\exp\left(\mathrm{j}2\pi\frac{\mathbf{r}_{\mathrm{rx},m}^j(t)\cdot\mathbf{R}_{\mathrm{rx}}(t)\cdot\mathbf{d}_{\mathrm{rx}}(t)}{\lambda}\right) \tag{5}$$
$$\cdot\exp\left(\mathrm{j}2\pi\frac{\mathbf{r}_{\mathrm{tx},m}^j(t)\cdot\mathbf{R}_{\mathrm{tx}}(t)\cdot\mathbf{d}_{\mathrm{tx}}(t)}{\lambda}\right)\exp\left(\frac{\mathrm{j}2\pi}{\lambda}\int_0^t f_m^j(t')\mathrm{d}t'\right)$$

where Φ_m represents the random initial phase distributed uniformly over $[0, 2\pi)$, λ is the wavelength, and $\mathbf{r}^j_{\mathrm{tx/rx},m}(t)$ and f^j_m denote the spherical unit vectors and Doppler frequency of mth ray, respectively, and can be further expressed as

$$\mathbf{r}^j_{\mathrm{tx/rx},m}(t) = \begin{bmatrix} \cos\beta^j_{\mathrm{tx/rx},m}(t)\cos\alpha^j_{\mathrm{tx/rx},m}(t) \\ \cos\beta^j_{\mathrm{tx/rx},m}(t)\sin\alpha^j_{\mathrm{tx/rx},m}(t) \\ \sin\beta^j_{\mathrm{tx/rx},m}(t) \end{bmatrix} \tag{6}$$

$$f^j_m(t) = \frac{\mathbf{v}_{\mathrm{tx}}(t)\cdot\mathbf{r}^j_{\mathrm{tx},m}(t) + \mathbf{v}_{\mathrm{rx}}(t)\cdot\mathbf{r}^j_{\mathrm{rx},m}(t)}{\lambda} \tag{7}$$

where $\alpha^j_{\mathrm{tx/rx},m}$ is the azimuth angle of departure (AAoD) or arrival (AAoA), and $\beta^j_{\mathrm{tx/rx},m}$ is the elevation angle of departure (EAoD) or arrival (EAoA).

The LoS path between UAV antenna and vehicle antenna can be viewed as a special case of NLoS path and can be expressed as

$$\begin{aligned} H^{\mathrm{LoS}}(t) = {} & \exp\left(-\mathrm{j}2\pi\frac{D_{\mathrm{LoS}}(t)}{\lambda}\right)\exp\left(\mathrm{j}2\pi\frac{\mathbf{r}^{\mathrm{LoS}}_{\mathrm{rx}}(t)\cdot\mathbf{R}_{\mathrm{rx}}(t)\cdot\mathbf{d}_{\mathrm{rx}}(t)}{\lambda}\right) \\ & \cdot\exp\left(\mathrm{j}2\pi\frac{\mathbf{r}^{\mathrm{LoS}}_{\mathrm{tx}}(t)\cdot\mathbf{R}_{\mathrm{tx}}(t)\cdot\mathbf{d}_{\mathrm{tx}}(t)}{\lambda}\right)\exp\left(\frac{\mathrm{j}2\pi}{\lambda}\int_0^t f^{\mathrm{LoS}}(t')dt'\right)\delta(t-\tau^{\mathrm{LoS}}(t)) \end{aligned} \tag{8}$$

where $D_{\mathrm{LoS}}(t)$ is the distance between the UAV and vehicle, $\mathbf{r}^{\mathrm{LoS}}_{\mathrm{tx/rx}}(t)$ and f^{LoS} denote the spherical unit vectors and Doppler frequency of LoS path, respectively. In (8), $\mathbf{r}^{\mathrm{LoS}}_{\mathrm{tx/rx}}(t)$ is determined by $\alpha^{\mathrm{LoS}}_{\mathrm{tx/rx}}$ and $\beta^{\mathrm{LoS}}_{\mathrm{tx/rx}}$ according to (6), and f^{LoS} can be obtained by $\mathbf{r}^{\mathrm{LoS}}_{\mathrm{tx/rx}}(t)$ according to (7).

3 Computation of Channel Parameters

3.1 Time-Variant Geometric Parameters

Since the UAV and vehicle move with 3D arbitrary trajectories, the time-variant location vector of UAV (or vehicle) can be expressed as

$$\mathbf{L}_{\mathrm{tx/rx}}(t) = \mathbf{L}_{\mathrm{tx/rx}}(t_0) + \int_{t_0}^{t}\mathbf{v}_{\mathrm{tx/rx}}(t)\mathrm{d}t \tag{9}$$

where $\mathbf{L}_{\mathrm{tx/rx}}(t_0)$ denotes the initial location vector of UAV (or vehicle) at $t = t_0$. Thus, the distance vector between the UAV and vehicle denoted as $\mathbf{D}_{\mathrm{LoS}}(t)$ or between UAV/vehicle and jth scatters denoted as $\mathbf{D}_{\mathrm{tx/rx},j}(t)$ can be expressed as

$$\mathbf{D}_{\mathrm{tx/rx,LoS}}(t) = \mathbf{L}_{\mathrm{tx/rx}}(t) - \mathbf{L}_{\mathrm{rx/tx}}(t) = D_{\mathrm{tx/rx,LoS}}(t_0)\mathbf{r}^{\mathrm{LoS}}_{\mathrm{tx/rx}}(t) + \int_{t_0}^{t}\mathbf{v}_{\mathrm{tx,rx}}(t)\mathrm{d}t \tag{10}$$

$$\mathbf{D}_{\mathrm{tx/rx},j}(t) = \mathbf{L}_{\mathrm{tx/rx}}(t) - \mathbf{L}_j(t) = D_{\mathrm{tx/rx},j}(t_0)\mathbf{r}^j_{\mathrm{tx/rx}}(t) + \textstyle\int_{t_0}^{t}\mathbf{v}_{\mathrm{tx/rx}}(t)\mathrm{d}t \tag{11}$$

where $\mathbf{v}_{tx,rx}(t)$ denotes the relative velocity between the UAV and vehicle, and $\mathbf{r}^j_{tx/rx}(t)$ is the spherical unit vectors of each NLoS path, which can be obtained by the mean angle parameters $\bar{\alpha}^j_{tx/rx}$ and $\bar{\beta}^j_{tx/rx}$ according to (6). Thus, the distance between UAV and vehicle in LoS scenario and the one between the UAV (or vehicle) and jth scatterer can be calculated by

$$D_{\mathrm{LoS}}(t) = \sqrt{\begin{array}{l}\left(\begin{array}{l}D_{\mathrm{tx/rx,LoS}}(t_0)\cos(\alpha^{\mathrm{LoS}}_{tx/rx}(t_0))\cos(\beta^{\mathrm{LoS}}_{tx/rx}(t_0))\\ +\int_{t_0}^{t}(v_{\mathrm{tx,rx}}(t))\cos(\alpha^{v}_{\mathrm{tx,rx}}(t))\cos(\beta^{v}_{\mathrm{tx,rx}}(t))dt\end{array}\right)^2\\ +\left(\begin{array}{l}D_{\mathrm{tx/rx,LoS}}(t_0)\cos(\beta^{\mathrm{LoS}}_{tx/rx}(t_0))\sin(\alpha^{\mathrm{LoS}}_{tx/rx}(t_0))\\ +\int_{t_0}^{t}(v_{\mathrm{tx,rx}}(t))\sin(\alpha^{v}_{\mathrm{tx,rx}}(t))\cos(\beta^{v}_{\mathrm{tx,rx}}(t))dt\end{array}\right)^2\\ +\left(\begin{array}{l}D_{\mathrm{tx/rx,LoS}}(t_0)\sin(\beta^{\mathrm{LoS}}_{tx/rx}(t_0))\\ +\int_{t_0}^{t}(v_{\mathrm{tx,rx}}(t))\sin(\beta^{v}_{\mathrm{tx,rx}}(t))dt\end{array}\right)^2\end{array}} \tag{12}$$

$$D_{\mathrm{tx/rx},j}(t) = \sqrt{\begin{array}{l}\left(\begin{array}{l}D_{\mathrm{tx/rx},j}(t_0)\cos(\bar{\alpha}^{j}_{tx/rx}(t_0))\cos(\bar{\beta}^{j}_{tx/rx}(t_0))\\ -\int_{t_0}^{t}(v_{\mathrm{tx/rx}}(t))\cos(\alpha^{v}_{\mathrm{tx/rx}}(t))\cos(\beta^{v}_{\mathrm{tx/rx}}(t))dt\end{array}\right)^2\\ +\left(\begin{array}{l}D_{\mathrm{tx/rx},j}(t_0)\cos(\bar{\beta}^{j}_{tx/rx}(t_0))\sin(\bar{\alpha}^{j}_{tx/rx}(t_0))\\ -\int_{t_0}^{t}(v_{\mathrm{tx/rx}}(t))\sin(\alpha^{v}_{\mathrm{tx/rx}}(t))\cos(\beta^{v}_{\mathrm{tx/rx}}(t))dt\end{array}\right)^2\\ +\left(\begin{array}{l}D_{\mathrm{tx/rx},j}(t_0)\sin(\bar{\beta}^{j}_{tx/rx}(t_0))\\ -\int_{t_0}^{t}(v_{\mathrm{tx/rx}}(t))\sin(\beta^{v}_{\mathrm{tx/rx}}(t))dt\end{array}\right)^2\end{array}} \tag{13}$$

where $\alpha^v_{\mathrm{tx,rx}}(t)$ and $\beta^v_{\mathrm{tx,rx}}(t)$ denote the relative travel direction between the UAV and vehicle on the azimuth and elevation plane, respectively.

3.2 Time-Variant Angle Parameters

Based on the geometric relationships, the time-variant angles such as the EAoD, AAoD, EAoA, and AAoA of LoS path under dynamic scattering scenarios can be expressed, respectively, as

$$\alpha^{\mathrm{LoS}}_{tx/rx}(t) = \begin{cases}\arccos(\frac{\left\|\mathbf{D}^x_{\mathrm{tx/rx,LoS}}(t)\right\|}{D_{\mathrm{LoS}}(t)}), \mathbf{D}^x_{\mathrm{tx/rx,LoS}}(t) \geq 0\\ \pi - \arccos(\frac{\left\|\mathbf{D}^x_{\mathrm{tx/rx,LoS}}(t)\right\|}{D_{\mathrm{LoS}}(t)}), \mathbf{D}^x_{\mathrm{tx/rx,LoS}}(t) < 0\end{cases} \tag{14}$$

$$\beta^{\mathrm{LoS}}_{tx/rx}(t) = \arcsin(\frac{\left\|\mathbf{D}^z_{\mathrm{tx/rx,LoS}}(t)\right\|}{D_{\mathrm{LoS}}(t)}) \tag{15}$$

where $\mathbf{D}^x_{\mathrm{tx/rx,LoS}}(t)$ denotes the x component of $\mathbf{D}_{\mathrm{tx/rx,LoS}}(t)$. Similarly, the mean angles of time-variant EAoD, AAoD or EAoA, AAoA for the NLoS paths can be calculated respectively by

$$\bar{\alpha}^j_{tx/rx}(t) = \begin{cases}\arccos(\frac{\left\|\mathbf{D}^x_{\mathrm{tx/rx},j}(t)\right\|}{D_{\mathrm{tx/rx},j}(t)}), \mathbf{D}^x_{\mathrm{tx/rx},j}(t) \geq 0\\ \pi - \arccos(\frac{\left\|\mathbf{D}^x_{\mathrm{tx,rx},j}(t)\right\|}{D_{\mathrm{tx/rx},j}(t)}), \mathbf{D}^x_{\mathrm{tx/rx},j}(t) < 0\end{cases} \tag{16}$$

$$\bar{\beta}^{j}_{\mathrm{tx/rx}}(t) = \arcsin\left(\frac{\left\|\mathbf{D}^{z}_{\mathrm{tx/rx},j}(t)\right\|}{D_{\mathrm{tx/rx},j}(t)}\right). \tag{17}$$

It should be mentioned that the angle of each ray within the NLoS path is random and cannot be calculated in a deterministic way. In this paper, we take the random factor into account and model them as the summation of a random offset angle and the mean angle of each path,

$$\alpha^{j}_{\mathrm{tx/rx},m}(t) = \bar{\alpha}^{j}_{\mathrm{tx/rx}}(t) + \Delta\alpha_m \tag{18}$$

$$\beta^{j}_{\mathrm{tx/rx},m}(t) = \bar{\beta}^{j}_{\mathrm{tx/rx}}(t) + \Delta\beta_m. \tag{19}$$

Based on the RT simulation results and measurement results in the 3GPP channel model, the offset angles $\Delta\alpha_m, \Delta\beta_m$ in this paper are obtained by generating a normal random variable with zero mean value and a Laplace distributed random variable, respectively.

3.3 Time-Variant Delays and Powers

The time-variant delays of LoS and NLoS paths are determined by the transmission distance and they can be calculated respectively by

$$\tau^{\mathrm{LoS}}(t) = \frac{D_{\mathrm{LoS}}(t)}{c} \tag{20}$$

$$\bar{\tau}^{j}(t) = \frac{D_{\mathrm{tx},j}(t) + D_{\mathrm{rx},j}(t)}{c} \tag{21}$$

where c is the speed of light. Furthermore, the delay of each ray within the NLoS path can be obtained by adding a random delay offset $\Delta\tau_m$ on the mean value of path delay as

$$\tau^{j}_{m}(t) = \bar{\tau}^{j}(t) + \Delta\tau_m. \tag{22}$$

The random delay offset $\Delta\tau_m$ is assumed to follow the exponential distribution and the corresponding power of each ray can be calculated by

$$P^{j}_{m}(t) = \exp\left(-\tau^{j}_{m}(t)\frac{1-r_\tau}{r_\tau\sigma_\tau}\right)10^{-\frac{Z_m}{10}} \tag{23}$$

where r_τ and σ_τ are the delay scalar and delay spread, respectively, and Z_m follows a Gaussian distribution $N(0,3)$. When the LoS power is normalized to be 0 dB, the ray powers can be normalized as

$$\tilde{P}^{j}_{m}(t) = \frac{P^{j}_{m}(t)}{K_R(t)\cdot\sum\limits_{m=1}^{M}P^{j}_{m}(t)} \tag{24}$$

Thus, the total power of NLoS paths should be $1/(K_R(t)+1)$ as shown in (3).

4 Simulation Results and Analysis

In this section, we simulate the proposed U2V channel model and compare the simulated results with the analytical and measured ones. In the simulation, the 3D time-variant velocities and directions of both terminals and 3D beam forming are considered. The detailed simulation parameters are given in Table 1. It should be mentioned that the effect of beam tracking error is not included. The beam width of UAV antenna array is assumed to be 30° while the one of vehicle antenna array is 180°.

Table 1. Simulation parameters.

Definition	Value	Definition	Value
$\|\mathbf{v}_{\mathrm{tx}}(t)\|$	$10 + 0.5t$ m/s	$\|\mathbf{v}_{\mathrm{rx}}(t)\|$	$2 + t$ m/s
$\alpha^v_{\mathrm{tx}}(t)$	$120 - 2t°$	$\beta^v_{\mathrm{tx}}(t)$	$6 + 5t°$
$\alpha^v_{\mathrm{rx}}(t)$	$-120 + 2t°$	$\beta^v_{\mathrm{rx}}(t)$	0°
f_0	28 GHz	K	7 dB
$\|\mathbf{L}_{\mathrm{tx}}(t_0)\|$	400 m	$\|\mathbf{L}_{\mathrm{rx}}(t_0)\|$	100 m

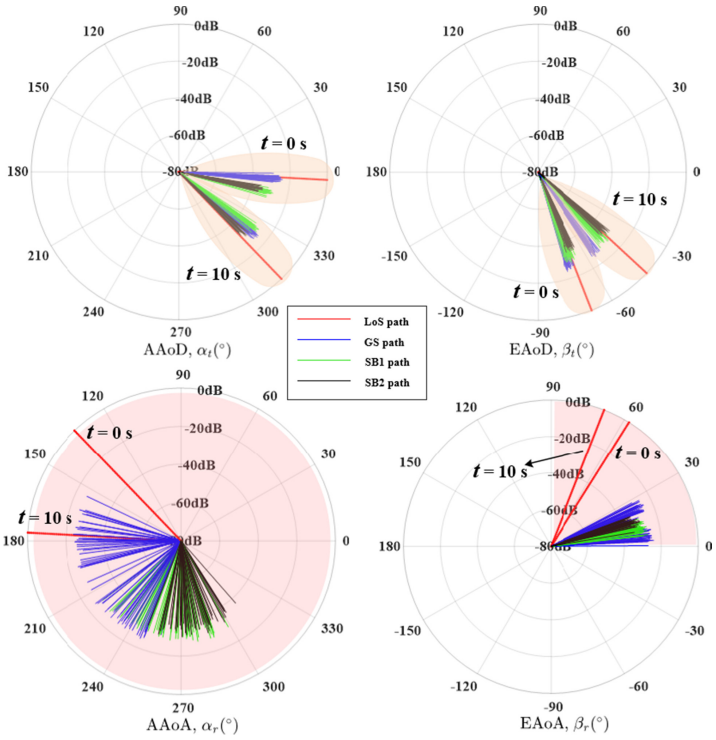

Fig. 2. The time-variant PAPs of LoS path and NLoS paths.

For the U2V mmWave beam channel, the angle parameters are more complicated and related with both the scattering scenario and beam width. Figure 2 gives the time-variant PAPs of LoS path and rays within three NLoS paths at two different time instants $t_1 = 0\,\mathrm{s}$ and $t_2 = 10\,\mathrm{s}$. As we can see, the AAoD and EAoD are limited within the beam and the beam changes to the desired direction at different time instants. In addition, the vehicle antenna is usually close to the ground and thus the EAoA ranges from $[0^\circ\ 90^\circ]$.

Based on the parameter computation method of (20)–(24), the delays and powers are calculated. The time-variant PDPs of proposed channel model are simulated and given in Fig. 3. In the figure, the delay and power of LoS path are both normalized and the number of intra-path rays is set as 32. As we can see that the power of each NLoS path and each intra-path rays show the trend of exponential decay with the increasement of relative delay.

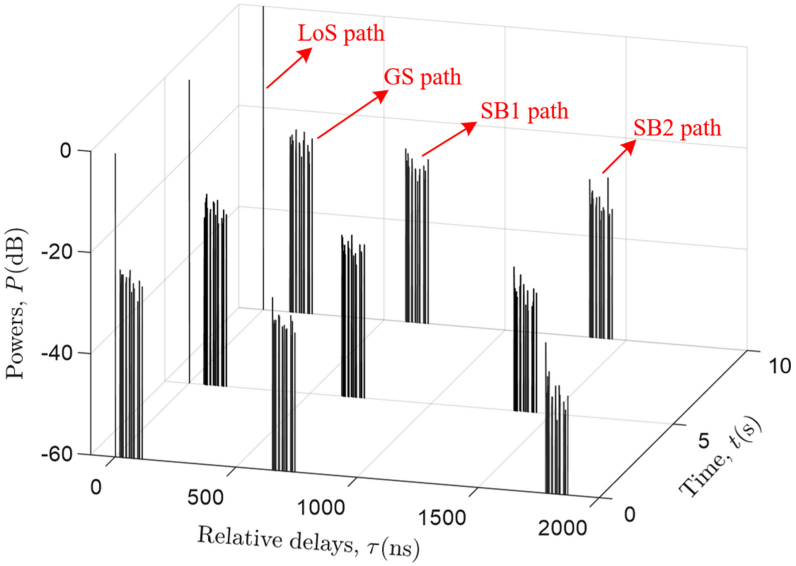

Fig. 3. The time-variant PDPs of proposed U2V channel.

In order to verify the correctness of proposed mmWave channel model, this paper focuses on analyzing and verifying two typical second order statistical properties, i.e., ACF and DPSD. The time-variant theoretical ACF of proposed model can be derived by substituting (3) into the ACF definition,

$$\rho\left(\Delta t; t\right) = E\left[H^*(t)H(t+\Delta t)\right] = \rho^{\mathrm{LoS}}\left(\Delta t; t\right) + \rho^{\mathrm{NLoS}}\left(\Delta t; t\right). \tag{25}$$

Considering the similar characteristic of each NLoS path, we only take the first one into account. The theoretical and simulated results of ACFs including the LoS path and first NLoS path are shown in Fig. 4. It shows that the ACFs change over time due to the time-variant channel parameters. Furthermore, we can get the time-variant DPSD by using the Fourier transform on the ACF. The simulated results are shown in Fig. 5, which also demonstrate that the Doppler frequency changes in a complicated way under the U2V communication scenario.

Finally, to further verify the consistency of proposed channel model with the realistic channel, the simulated ACFs are compared with the field-measured ones in [28]. To the best of our knowledge, there are very few literatures involving UAV mmWave channel measurement [25,29,30] and none of them so far analyzed the measured ACFs. Since the proposed model is compatible for the sub-mmWave channel by adjust some channel parameters. The measured ACF of sub-mmWave channel in [28] is chose. The beam width is ignored and some simulation parameters are configured as $f_0 = 2\,\text{GHz}$, $\|\mathbf{L}_{\text{tx}}(t_0)\| = 300\,\text{m}$, and $\|\mathbf{v}_{\text{rx}}(t)\| = 1.2\,\text{m/s}$. The comparison result is given in Fig. 6 which shows a good agreement between the simulated result and the measured one.

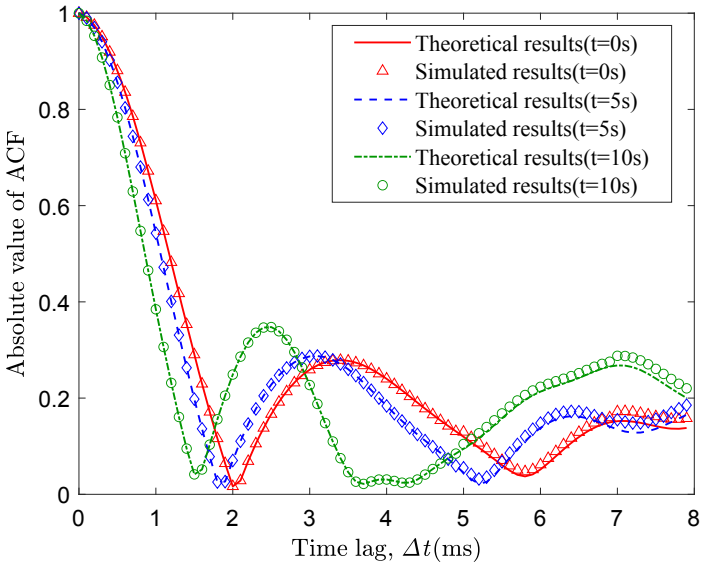

Fig. 4. The simulated and theoretical time-variant ACFs at three time instants.

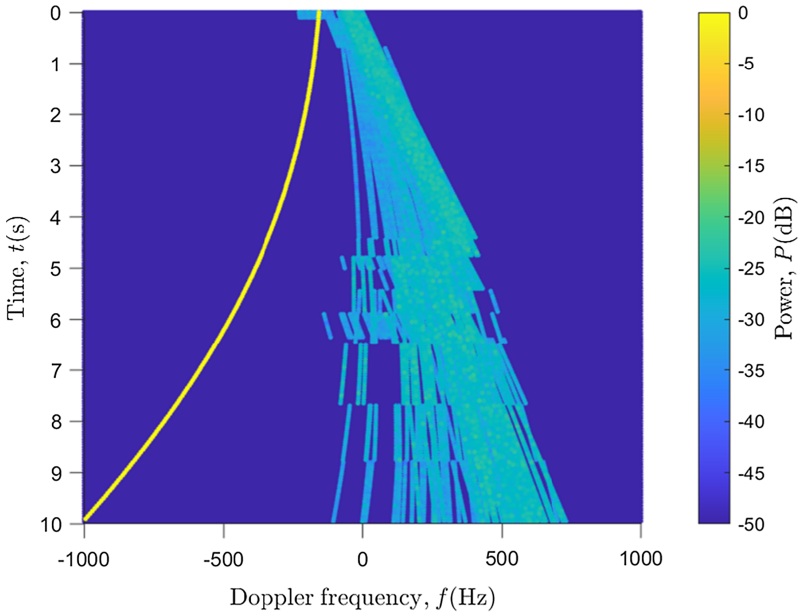

Fig. 5. The simulated time-variant DPSDs.

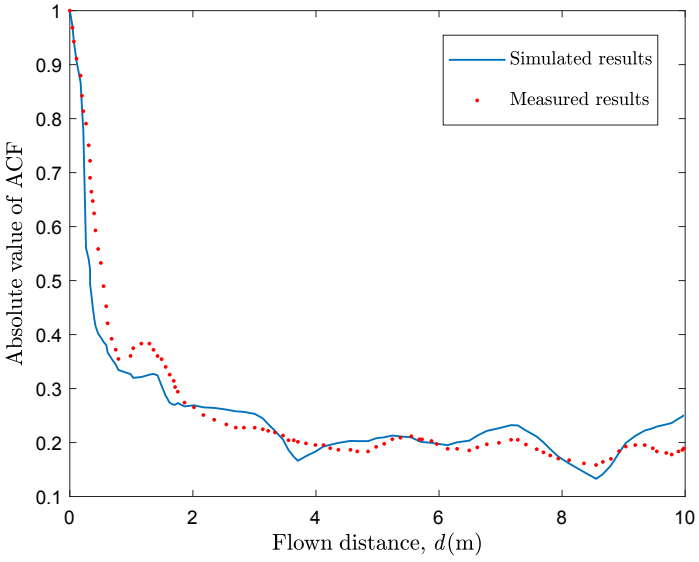

Fig. 6. The simulated and measured ACFs.

5 Conclusions

This paper has proposed a U2V mmWave channel model by considering the 3D trajectory of UAV and vehicle, 3D antenna array, and 3D directional beam. In order to achieve the tradeoff between complexity and precision, only the LoS path and three strongest NLoS paths have been included in the new model. Moreover, the computation method of channel parameters have also been given. It is divided into a deterministic part and a stochastic part to guarantee both the correctness and efficiency. Finally, the statistical characteristic of PDP, ACF, and DPSD have been simulated, analyzed and compared with the theoretical and measured ones. In the future, we will perform more channel measurements as well as apply the proposed model to the optimization of beam-forming and tracking algorithms for UAV mmWave communications.

Acknowledgements. This work was supported in part by the National Key Scientific Instrument and Equipment Development Project under Grant No. 61827801, in part by Aeronautical Science Foundation of China, No. 201901052001 and No. 2017ZC52021, in part by the Fundamental Research Funds for the Central Universities, No. NS2020026 and No. NS2020063.

References

1. Zhang, L., Zhao, H., Hou, S., Zhao, Z., Xu, H., et al.: A survey on 5G millimeter wave communications for UAV-assisted wireless networks. IEEE Access **7**, 117460–117504 (2019)
2. Li, B., Fei, Z., Zhang, Y.: UAV communications for 5G and beyond: recent advances and future trends. IEEE Internet Things J. **6**(2), 2241–2263 (2018)
3. Zhong, W., Xu, L., Zhu, Q., Chen, X., Zhou, J.: MmWave beamforming for UAV communications with unstable beam pointing. China Commun. **16**(1), 37–46 (2019)
4. Zhong, W., Xu, L., Liu, X., Zhu, Q., Zhou, J.: Adaptive beam design for UAV network with uniform plane array. Phys. Commun. **34**(2), 58–65 (2019)
5. Khawaja, W., Guvenc, I., Matolak, D.W., Fiebig, U., Schneckenburger, N.: A survey of air-to-ground propagation channel modeling for unmanned aerial vehicles. IEEE Commun. Surv. Tuts. **21**(3), 2361–2391 (2019)
6. Zhang, C., Zhang, W., Wang, W., Yang, L., Zhang, W.: Research challenges and opportunities of UAV millimeter-wave communications. IEEE Wireless Commun. **26**(1), 58–62 (2019)
7. Cui, Z., Briso-Rodrguez, C., Guan, K., Calvo-Ramrez, C., Ai, B., Zhong, Z.: Measurement-based modeling and analysis of UAV air-ground channels at 1 and 4 GHz. IEEE Antennas Wirel. Propag. Lett. **18**(9), 1804–1808 (2019)
8. Chu, X., Briso, C., He, D., Yin, X., Dou, J.: Channel modeling for low-altitude UAV in suburban environments based on ray tracer. In: Proceedings of the EuCAP 2018, London, UK, pp. 1–4, April 2018
9. Zhu, Q., Wang, Y., Jiang, K., Chen, X., Zhong, W., Ahmed, N.: 3D non-stationary geometry-based multi-input multi-output channel model for UAV-ground communication systems. IET Microw. Antennas Propag. **13**(8), 1104–1112 (2019)

10. Chang, H., Bian, J., Wang, C.-X., Aggoune, E.M.: A 3D non-stationary wideband GBSM for low-altitude UAV-to-ground V2V MIMO channels. IEEE Access **7**, 70719–70732 (2019)
11. Zhang, X., Cheng, X.: Three-dimensional non-stationary geometry-based stochastic model for UAV-MIMO Ricean fading channels. IET Commun. **13**(16), 2617–2627 (2019)
12. Zhu, Q., Jiang, K., Chen, X., Zhong, W., Yang, Y.: A novel 3D non-stationary UAV-MIMO channel model and its statistical properties. China Commun. **15**(12), 147–158 (2018)
13. Chen, X., Hu, X., Zhu, Q., Zhong, W., Chen, B.: Channel modeling and performance analysis for UAV relay systems. China Commun. **15**(12), 89–97 (2018)
14. Huang, J., Liu, Y., Wang, C.-X., Sun, J., Xiao, H.: 5G millimeter wave channel sounders, measurements, and models: recent developments and future challenges. IEEE Commun. Mag. **57**(1), 138–145 (2019)
15. Gonzlez-Plaza, A., Calvo-Ramrez, C., Briso-Rodrguez, C., Garca-Loygorri, J.M., Oliva, D., Alonso, J.I.: Propagation at mmW band in metropolitan railway tunnels. Wireless Commun. Mobile Computing **2018**, 1–10 (2017)
16. Liu, X., Yin, X., Zheng, G.: Experimental investigation of millimeter-wave MIMO channel characteristics in tunnel. IEEE Access **7**, 108395–108399 (2019)
17. He, R., Ai, B., Stber, G.L., Wang, G., Zhong, Z.: Geometrical-based modeling for millimeter-wave MIMO mobile-to-mobile channels. IEEE Trans. Veh. Technol. **67**(4), 2848–2863 (2018)
18. Bas, C.U., Wang, R., Sangodoyin, S., Hur, S., Whang, K., et al.: 28 GHz propagation channel measurements for 5G microcellular environments. In: Proceedings of the ACES 2018, Denver, CO, pp. 1–2 (2018)
19. Wang, C.-X., Bian, J., Sun, J., Zhang, W., Zhang, M.: A survey of 5G channel measurements and models. IEEE Commun. Surv. Tuts. **20**(4), 3142–3168 (2018)
20. Fan, W., Carton, I., Kyosti, P., Karstensen, A., Jamsa, T., et al.: A step toward 5G in 2020: low-cost OTA performance evaluation of massive MIMO base stations. IEEE Antennas Propag. Mag. **59**(1), 38–47 (2017)
21. Zhang, J., Shafi, M., Molisch, A., Tufvesson, F., Wu, S., et al.: Channel models and measurements for 5G. IEEE Commun. Mag. **56**(12), 12–13 (2018)
22. Fu, Z., Cui, H., Geng, S., Zhao, X.: 5G millimeter wave channel modeling and simulations for a high-voltage substation. In: Proceedings of the iSPEC 2019, Beijing, China, pp. 1822–1826 (2019)
23. Yang, G., Zhang, Y., He, Z., Wen, J., Ji, Z., Li, Y.: Machine-learning-based prediction methods for path loss and delay spread in air-to-ground millimetre-wave channels. IET Microw. Antennas Propag. **13**(8), 1113–1121 (2019)
24. Khawaja, W., Ozdemir, O., Guvenc, I.: Temporal and spatial characteristics of mm wave propagation channels for UAVs. In: Proceedings of the GSMM 2018, Boulder, CO, USA, pp. 1–6, May 2018
25. Geise, R., Weiss, A., Neubauer, B.: Modulating features of field measurements with a UAV at millimeter wave frequencies. In: Proceedings of the CAMA 2018, Vasteras, Sweden, pp. 1–4, September 2018
26. Michailidis, E.T., Nomikos, N., Trakadas, P., Kanatas, A.G.: Three-dimensional modeling of mmWave doubly massive MIMO aerial fading channels. IEEE Trans. Veh. Technol. **69**(2), 1190–1202 (2020)
27. Cheng, L., Zhu, Q., Wang, C.-X., Zhong, W., Hua, B., Jiang, S.: Modeling and simulation for UAV air-to-ground mmWave channels. In: Proceedings of the EuCAP 2020, Copenhagen, pp. 1–5, March 2020

28. Simunek, M., Fontn, F.P., Pechac, P.: The UAV low elevation propagation channel in urban areas: statistical analysis and time-series generator. IEEE Trans. Antennas Propag. **61**(7), 3850–3858 (2013)
29. Lemos Cid, E., Alejos, A.V., Garcia Sanchez, M.: Signaling through scattered vegetation: empirical loss modeling for low elevation angle satellite paths obstructed by isolated thin trees. IEEE Veh. Technol. Mag. **11**(3), 22–28 (2016)
30. Khawaja, W., Ozdemir, O., Guvenc, I.: UAV air-to-ground channel characterization for mmWave systems. In: Proceedings of the VTC 2017, Toronto, ON, pp. 1–5 (2017)